Journal of Alloys and Compounds 509 (2011) 7373–7380

Contents lists available at ScienceDirect

Journal of Alloys and Compounds

journal homepage: www.elsevier.com/locate/jallcom

Review

Structural impact of tungsten ions on $ZnO–Sb_2O_3–As_2O_3$ glass system

S. Bala Murali Krishna, D. Krishna Rao*

Department of Physics, Acharya Nagarjuna University, Nagarjuna Nagar, Guntur 522 510, Andhra Pradesh, India

ARTICLE INFO

Article history:
Received 14 March 2011
Received in revised form 18 April 2011
Accepted 19 April 2011
Available online 27 April 2011

Keywords:
Amorphous materials
Rapid-solidification
Quenching
Dielectric response
Optical properties
Electron paramagnetic resonance
X-ray diffraction

ABSTRACT

Five glasses in the quaternary system 5 ZnO–(50 − *x*) As_2O_3–45 Sb_2O_3 : *x* WO_3 with the values of *x* ranging from 0 to 20 mol% (in steps of 5 mol%) are prepared. The samples are characterized by X-ray diffraction, scanning electron microscopy, energy dispersive spectroscopy (EDS) and differential thermal analysis (DTA) techniques. The DTA studies have indicated that the glass forming ability decreases with the increasing content of WO_3. A number of studies, like, spectroscopic (optical absorption, IR, Raman, ESR spectra) and dielectric studies (dielectric constant ε, loss tan δ, a.c. conductivity $\sigma_{a.c.}$) over a wide range of frequency and temperature and dielectric break down strength at room temperature, have been carried out and are analysed in the light of different oxidation states and environment of tungsten ions in these glasses. These glasses have potential photonic applications.

Contents

1. Introduction

Tungsten ions are expected to have profound influence on the physical properties of antimony arsenate glasses, for the simple reason that the tungsten ions exist in different valance states viz., W^{6+}, W^{5+} and also in W^{4+} state, regardless of the oxidation state of the tungsten ion in the starting glass batch [1–4] as per the following thermo reversible disproportionate reaction:

$$W^{5+} + W^{5+} \leftrightarrow W^{4+} + W^{6+}$$

Tungsten oxide participates in the glass network with different structural units like WO_4 (Td) and WO_6 (Oh) of W^{6+} ions and $W^{5+}O_3^-$ (Oh) of W^{5+}ions [5]. The concentration of different structural groups of tungsten ions with different oxidation states present in the glass matrix at a given temperature depends on the quantitative properties of modifiers, glass formers, size of ions in the glass structure, mobility of the modifier cation etc. W^{5+} ions are well known paramagnetic ions. The presence of tungsten in antimony arsenate glasses, further, makes the glasses suitable for optoelectronic devices since they exhibit photochromism and electrochromism properties [6,7]. The structural groups of tungsten oxide are expected to alternate with AsO_3, AsO_4 and SbO_3 structural groups and are likely to influence the physical properties of antimony arsenate glasses to a large extent (since some of the vibrational modes of these groups lie in the region of SbO_3 and AsO_3 structural groups). The presence of metal oxide like ZnO, between the long chain molecules in the vicinity of tungsten ions in the antimony arsenate network, the symmetry and/or covalency of the glass at the W^{6+} ions will be varied. Additionally, the variations in the oxidation states of antimony ions are also expected to modify the crystal field around tungsten ions in the host glass network. As a result, the structural probing of tungsten ions on

* Corresponding author. Tel.: +91 863 6458142 (R)/2346380 (O); fax: +91 863 2293378.
E-mail addresses: krdhanekula@yahoo.co.in, sbmkkrishna@yahoo.co.in (D. Krishna Rao).

0925-8388/$ – see front matter © 2011 Elsevier B.V. All rights reserved.
doi:10.1016/j.jallcom.2011.04.100

$ZnO–Sb_2O_3–As_2O_3$ (ZAS) glass network is expected to be highly interesting and useful for the practical applications of these glasses. Thus, the objective of the present study is to investigate the structural changes that take place with the varied oxidation states of tungsten ions in $ZnO–Sb_2O_3–As_2O_3$ glass network by a systematic study on dielectric properties (viz., dielectric constant, loss and a.c. conductivity over a wide range of frequency and temperature, dielectric breakdown strength at room temperature), ESR, optical absorption, IR and Raman spectral studies etc.

2. Materials and methods

The starting materials are ZnO, As_2O_3, Sb_2O_3, WO_3 powders of the analytical reagent grade chemicals. Taking appropriate amounts (all in mol%) of these chemicals, mixing them thoroughly in an agate mortar and melted the mixture in a thick walled platinum crucible in the temperature range of 1000–1050 °C in a PID temperature controlled furnace for about 15 min until bubble free liquid was formed. The resultant melt was then poured on a brass mould and subsequently annealed at 350 °C. Transparent yellow colored glasses are obtained.

3. Experimental

Five glasses in the quaternary system 5 ZnO–$(50 - x)$ As_2O_3–45 Sb_2O_3: x WO_3 with the values of x ranging from 0 to 20 mol% (in steps of 5 mol%) are synthesized. The details of the composition are as follows.

W-0 : $5ZnO–50As_2O_3–45Sb_2O_3$

W-5 : $5ZnO–45As_2O_3–45Sb_2O_3$: $5WO_3$

W-10 : $5ZnO–40As_2O_3–45Sb_2O_3$: $10WO_3$

W-15 : $5ZnO–35As_2O_3–45Sb_2O_3$: $15WO_3$

W-20 : $5ZnO–30As_2O_3–45Sb_2O_3$: $20WO_3$

The amorphous nature of the glasses was confirmed by X-ray diffraction spectra recorded on SEIFERT diffractometer model SO-DEBYE FLUX 202 fitted with copper target and nickel filter operated at 40 kV and 30 mA. To check the crystallinity, if any, in the samples scanning electron microscopy (SEM) studies are also carried out on these glasses using Carl Zeiss, EVO MA 15, OXFORD INSTRUMENTES, Inca Penta FET x3 Scanning Electron Microscope. Differential thermal analysis of all the samples is carried out using METTLER STAR^e SW 8.10 instrument (to an accuracy of ±1 °C) with a programmed heating rate of 10 °C/min, in the temperature range 30–1200 °C. The density d of the glasses is determined to an accuracy of ±0.0001, by the standard principle of Archimedes' using o-Xylene (99.99% pure) as the buoyant liquid.

The IR spectra of the glasses are recorded by KBr pellet method. Glass powders (2 mg) are mixed with anhydrous potassium bromide powder (150 mg) and pressed into pellets at 2000 kg/cm^2. The spectra are recorded using PERKIN-ELMER Spectrum BX FT IR system spectrophotometer in the range 400–2000 cm^{-1} with a spectral resolution of 0.1 cm^{-1}. Micro Raman spectra are recorded using a Horiba Jobin-Yvon-UV800 Lab Ram HR spectrometer with a 17 mW internal He–Ne (helium–neon) laser source of excitation wavelength 632.8 nm with a spectral resolution of about ~0.33 cm^{-1}. The EPR spectra have been recorded at room temperature using a JEOL–FE1X EPR spectrometer operating in the X-band frequency (9.205 GHz) with a field modulation frequency of 100 kHz. The magnetic field was scanned from 0 to 5000 G and the microwave power used was 5 mW. A powdered glass specimen of 100 mg is taken in a quartz tube for EPR measurements.

For optical and dielectric studies the glasses are ground flat and circular shaped to a diameter of about 2 cm and to a thickness of about 0.2 cm. The optical absorption spectra of the glasses are recorded at room temperature in the wavelength range 200–900 nm up to a resolution of 0.5 nm using JASCO V-670 UV–Vis spectrophotometer. A thin layer of silver paint is applied on either side of the large-faces of the samples, in order to serve as electrodes for the dielectric measurements. Using LF-Impedance analyzer (Hewlett–Packard model 4192A) in the frequency range 10^3–10^6 Hz, the dielectric constant and dielectric loss are measured in the temperature range 30–300 °C. The accuracy in the measurement of dielectric constant is ~0.001 and that of loss is ~0.0001. Dielectric breakdown strength for all the glasses is determined at room temperature in air medium using a high a.c. voltage breakdown tester (ITL Model BDV-7, Hyderabad) operated with an input voltage of 230 V ± 10% at a frequency of 50 Hz; it is ensured that all the glasses used for this study are of almost identical thickness.

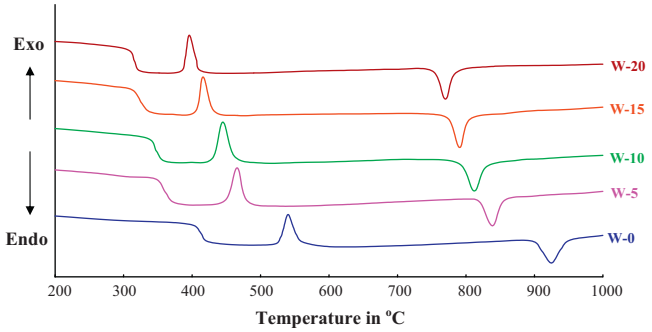

Fig. 1. DTA patterns of $ZnO–As_2O_3–Sb_2O_3$: WO_3 glasses.

4. Results

The chemical makeup of the samples is characterized by energy dispersive spectroscopy (EDS); the analysis indicates the presence of O, As, Sb, Zn and W elements in these glasses. The X-ray diffraction patterns and scanning electron micrograms of the samples confirm the amorphous nature. From the measured values of the density d and calculated average molecular weight $\overline{M}$, various physical parameters such as tungsten ion concentration N_i, mean tungsten ion separation R_i, polaron radius R_p that are useful for understanding physical properties of the glasses are evaluated and presented in Table 1.

Fig. 1 represents DTA traces of $ZnO–As_2O_3–Sb_2O_3$: WO_3 samples. These thermograms indicate typical glass transitions with the inflection point between 413 and 316 °C. The glass transitions temperature (T_g) shows decreasing trend with increase in the content of WO_3 (Table 1). In the high temperature part of the DTA traces, at about 450 °C a well-defined exothermic effect due to crystallization temperature (T_c) followed by an endothermic effect due to re-melting of the glasses can be visualized. The difference between T_c and T_g is observed to decrease with increase in the concentration of WO_3. From the measured values of T_g, T_c and T_m, the glass forming ability parameter, known as Hruby's parameter, $K_{gl} = (T_c - T_g)/(T_m - T_c)$, is evaluated and its variation with the increasing concentration of tungsten ions is found to decrease (Table 1).

The optical absorption spectra of $ZnO–As_2O_3–Sb_2O_3$ glasses encompassing various amounts of WO_3, recorded at room temperature in the wavelength region 400–500 nm are shown in Fig. 2. With the addition of WO_3 the absorption edge observed at 418 nm for the glass free from tungsten ions (W-0) is found to be shifted gradually towards higher wavelength. From the observed absorption edges, we have evaluated the optical band gap (E_o) of these glasses by drawing Urbach plot between ($h\upsilon$) and $(\alpha h\upsilon)^2$ as per the equation

$$\alpha(\upsilon)h\upsilon = c(h\upsilon - E_o)^n, \quad (1)$$

A considerable part of such plot of each glass is observed to be linear. The values of optical band gap (E_o) obtained from the extrapolation of linear portions of the plots are furnished in Table 1; with an increase in the content of WO_3, the value of E_o is found to decrease (inset (a) of Fig. 2) gradually from 2.68 eV (for glass W-0) to 2.51 eV (glass W-20). Additionally, spectra of all the glasses doped with tungsten ions exhibited a broad absorption band with a peak at about 828 nm (W-5); with the increasing concentration of WO_3 the half width and the intensity of the peak is observed to increase (inset (b) of Fig. 2).

Fig. 3 represents the IR transmission spectra of $ZnO–As_2O_3–Sb_2O_3$: WO_3 glasses. The spectrum of the glass, free from WO_3 (W-0) exhibited four absorption bands (i) at about 948 cm^{-1} due to υ_1 vibrations of Sb_2O_3, (ii) 770 cm^{-1} common

Table 1
Summary of data on various physical parameters of ZAS: WO_3 glasses.

Property	W-0	W-5	W-10	W-15	W-20
Avg. molecular weight (±0.01) g/mol	234.16	235.86	237.57	239.27	240.97
Density d (±0.0001) g/cc	4.70	4.87	5.04	5.21	5.39
Conc. W ions $N_i \times 10^{21}/(cm^3)$ (±0.01)	–	0.62	1.28	1.97	2.69
W ion separation R_i (±0.01) (Å)	–	11.73	9.22	7.98	7.19
Polaron radius R_p (±0.01) (Å)	–	4.73	3.71	3.22	2.90
Glass transition temp. T_g (±1) (°C)	413	361	348	327	316
Hruby's parameter K_{gl} (±0.0001)	0.3299	0.2815	0.2643	0.2373	0.2139
Cut-off wavelength λ (±0.5) (nm)	418	433	443	451	455
Optical band gap E_o (±0.01) (eV)	2.68	2.64	2.59	2.54	2.51
Band position (±0.5) (nm)	–	828	836	842	845

meta centre owing to the υ_3 vibrations of As_2O_3 and Sb_2O_3, (iii) 650 cm^{-1} common meta centre owing to the υ_2 vibrations of As_2O_3 and Sb_2O_3, and (iv) 554 cm^{-1} common meta centre owing to the υ_4 vibrations of As_2O_3 and Sb_2O_3. In the region of υ_4 vibrations it is also quite likely that the vibrations due to ZnO_4 structural units are also present. The spectra of the glasses containing WO_3 exhibited two additional bands, one at about 965 cm^{-1} and the other around 445 cm^{-1}, identified due to υ_3 and υ_4 vibrations of WO_6 and WO_4 structural units respectively [8,9]. From the spectra, it is clear that with increasing concentration of tungsten ions in the glass matrix the intensity of the band around 972 cm^{-1} is found to increase with a shift towards lower wavenumber. Though, the introduction of WO_3 into the ZAS glass shifted the band at 948 cm^{-1} towards lower wavenumber but the increasing content of WO_3 shifted this band towards higher wavenumber with decreasing intensity. All the other bands are found to be shifted towards higher wavenumber with decreasing intensity. Summary of the data on IR band positions is presented in Table 2.

The shape of Raman spectra of the glasses under study is strongly influenced by the presence of tungsten oxide in (Fig. 4). Apart from various conventional asymmetric/deformed modes of vibrations of As_2O_3 and Sb_2O_3, the spectra exhibited a central band around 440 cm^{-1}, attributed to the common mode of symmetric stretching vibrations of AsO_3 pyramids, SbO_3 pyramids and ZnO_4 structural units [10–13]. Inclusion of WO_3 into the ZAS glass matrix resulted new bands at about 963, 938 and 360 cm^{-1}. These bands can

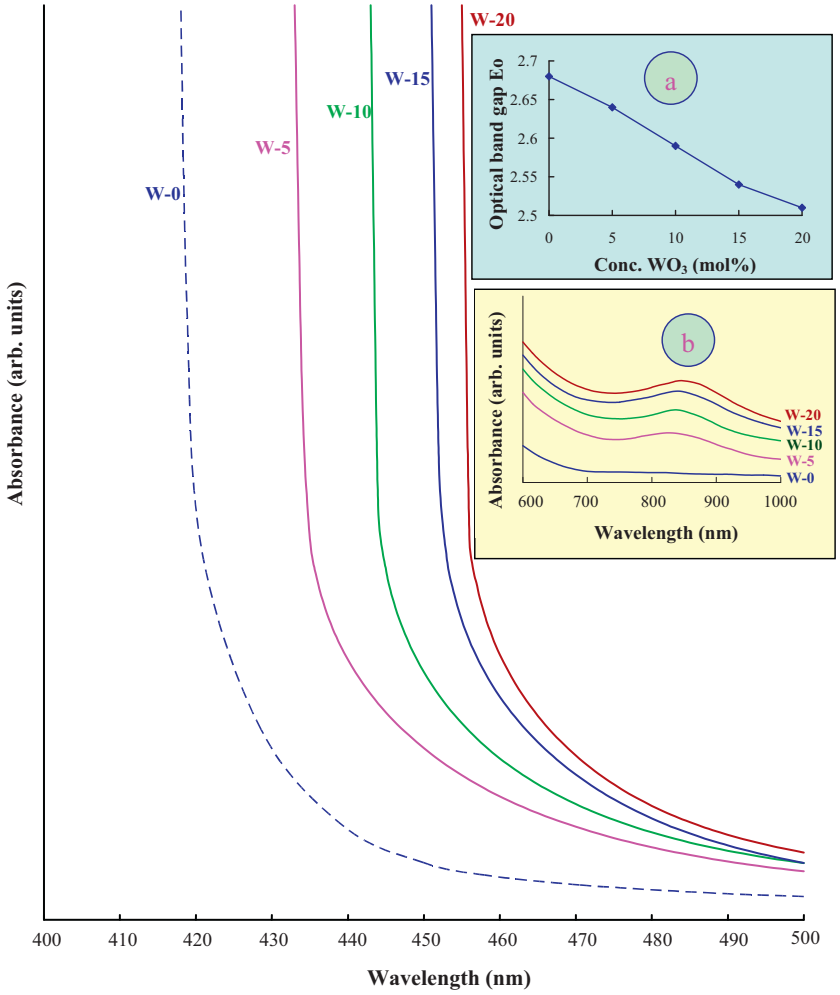

Fig. 2. Optical absorption spectra of $ZnO–As_2O_3–Sb_2O_3$: WO_3 glasses. Inset (a) represents the variation of optical band gap of the glasses with WO_3 concentration and (b) represents the absorption bands of ZAS: WO_3 glasses.

Table 2
Summary of the data on IR band positions in cm^{-1} of ZAS: WO_3 glasses.

Structural groups	W-0	W-5	W-10	W-15	W-20
υ_1-Sb_2O_3 symmetric stretching/W–O–W stretching	948	930	933	936	941
υ_3-As_2O_3 and υ_3-Sb_2O_3 doubly degenerate stretching	770	776	780	784	787
υ_2-As_2O_3 and υ_2-Sb_2O_3 symmetric bending	650	657	662	665	668
υ_4-As_2O_3, υ_4-Sb_2O_3 doubly degenerate bending and ZnO_4 structural units	554	556	557	558	559
υ_3-WO_6 structural units	–	972	969	967	965
υ_4-WO_4 structural units	–	430	436	441	445

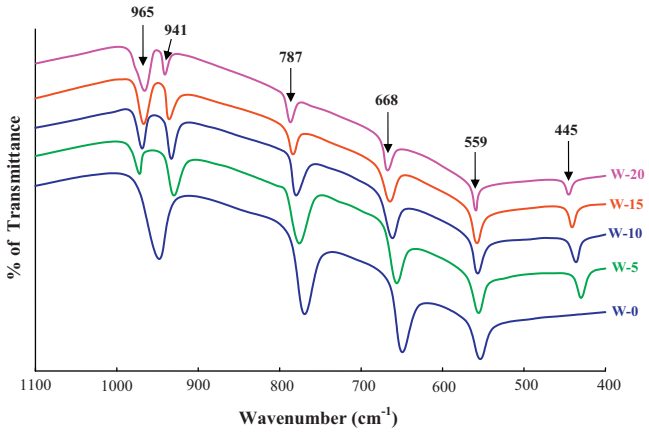

Fig. 3. IR spectra of ZAS glasses containing different concentrations of WO_3.

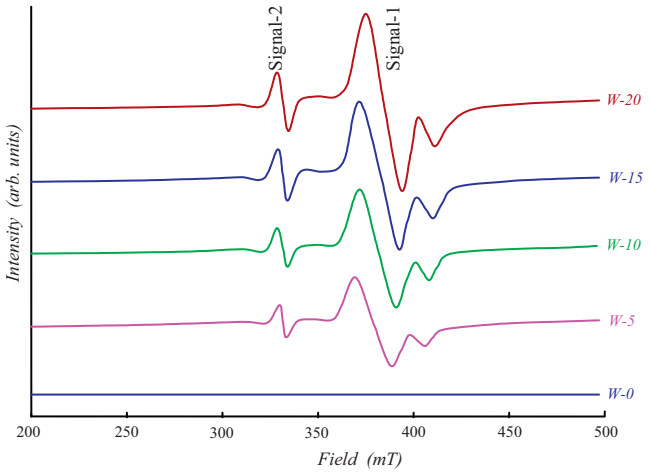

Fig. 5. ESR spectra of ZAS: WO_3 glasses recorded at room temperature.

be assigned to the stretching vibrations of W–O^- bonds [14–17], asymmetric stretching vibrations of terminal W–O bonds in WO_6 octahedra [15,18] and bending vibrations of W–O terminal bonds in WO_6 octahedra [19] respectively. Further, with the introduction of WO_3 into the ZAS glass matrix, the band due to stretching vibrations of arsenic and antimony (739–745 cm^{-1}) is found to be shifted towards lower wavenumber with slight increase in its intensity. But, thereafter, the increasing amount of WO_3 resulted an ongoing decrease in the intensity of this band by gradually shifting it towards higher wavenumber. This can be attributed to the formation of As–O–W or Sb–O–W or both, since the stretching vibrations of W–O–W are also present in this region (739–745 cm^{-1}). Overall, with the increasing content of WO_3, the specific bands of WO_6 are observed to grow in intensity and finally became dominant features of the spectrum. Summary of the pertinent data on Raman spectra of these glasses is presented in Table 3.

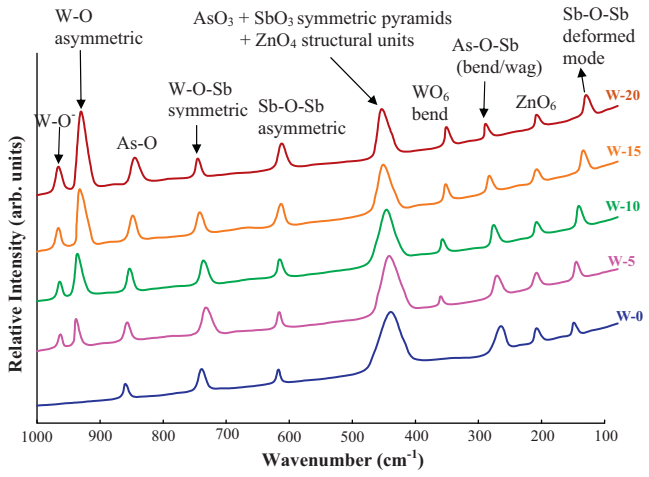

Fig. 4. Raman spectra of ZnO–As_2O_3–Sb_2O_3: WO_3 glasses.

The ESR spectra (at room temperature) of the glasses under study are presented in Fig. 5. The glass free from WO_3 did not exhibit any signal, while the glasses having WO_3 displayed two signals, an asymmetric signal (signal-1) identified due to W^{5+} ions and the other (signal-2) identified due to oxygen (paramagnetic O^-) ions defects [20]. The intensity of these signals is observed to be increasing with the increasing content of WO_3. From the spectra $g_{||}$ and $g_{\perp}$ values are evaluated using which the covalency reduction factors $k_{||}$ and $k_{\perp}$ are obtained and are presented in Table 4.

Table 3
Band positions (in cm^{-1}) in the Raman spectra of ZnO–As_2O_3–Sb_2O_3: WO_3 glasses.

Glass	AsO_3, SbO_3 and ZnO_4 units [7]	ZnO_6 units [9,10]	Arsenate groups (As–O–As) [11,12]			Antimony groups [13–15]		Tungsten oxide groups [16,17]		
			Asymmetric	Symmetric	Bend/wag	Sb–O–Sb asymmetric	Deformed mode	W–O^- of WO_6	W–O asymmetric of WO_6	W–O bend of WO_6
W-0	440	208	860	739	265	617	149	–	–	–
W-5	442	208	857	732	271	616	145	966	938	360
W-10	446	208	853	736	276	615	141	965	936	357
W-15	451	208	848	742	283	613	134	963	932	352
W-20	454	208	845	745	289	612	129	962	930	351

Table 4
Summary of the data on ESR spectra of ZAS: WO_3 glasses.

Glass	$g_\perp$	$g_\parallel$	$k_\perp$	$k_\parallel$
W-5	1.736	1.633	0.697	0.456
W-10	1.725	1.624	0.712	0.461
W-15	1.717	1.618	0.722	0.464
W-20	1.711	1.614	0.729	0.467

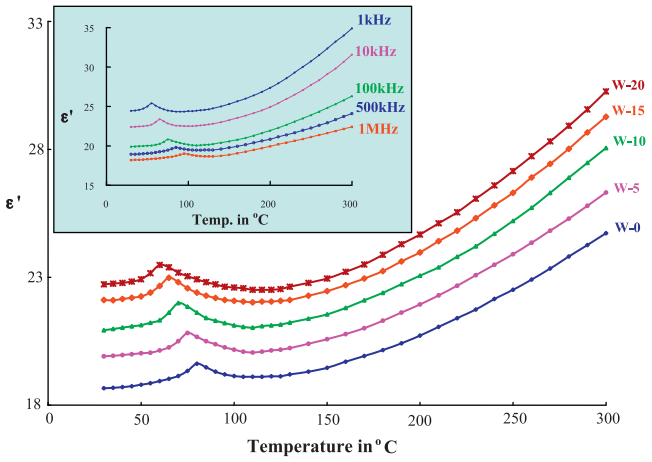

Fig. 6. Variation of dielectric constant ε' with temperature at 100 kHz for different concentrations of WO_3 in ZnO–As_2O_3–Sb_2O_3 glasses. Inset figure gives the variation of ε' of the glass W-5 with temperature at different frequencies.

The dielectric constant ε' and loss $\tan\delta$ at room temperature (≈30 °C) of the sample W-0 (WO_3 free ZnO–As_2O_3–Sb_2O_3 glass) at 1 MHz are measured to be 17.38 and 0.002846 respectively; the values of these parameters are found to increase considerably with decrease in frequency. With the addition of WO_3 into the glass matrix, the dielectric constant ε' and loss measured at room temperature are found to increase for any frequency. The temperature dependence of ε' for different concentrations of WO_3, measured at 100 kHz is shown in Fig. 6 and for a particular glass W-5 (containing 5 mol% of WO_3) at different frequencies is shown as the inset of Fig. 6. The value of ε' is found to exhibit a considerable increase at higher temperatures especially at lower frequencies.

The variation of dielectric loss with the concentration of WO_3 measured at room temperature has exhibited a similar behavior as that of ε'. The temperature dependence of $\tan\delta$ of the glass W-20 measured at different frequencies is presented in Fig. 7. Inset of the same figure represents the variation of $\tan\delta$ with temperature of all the glasses measured at a frequency of 10 kHz. The curves of both pure and WO_3 doped ZAS glasses have exhibited distinct maxima; with increasing frequency the temperature maximum shifts towards higher temperature and with increasing temperature the frequency maximum shifts towards higher frequency, indicating the dielectric relaxation character of dielectric loss of these samples. The observations on the variation of dielectric loss with temperature for different concentrations of WO_3 further indicates a gradual decrease in the broadness and $(\tan\delta)_{max}$ of

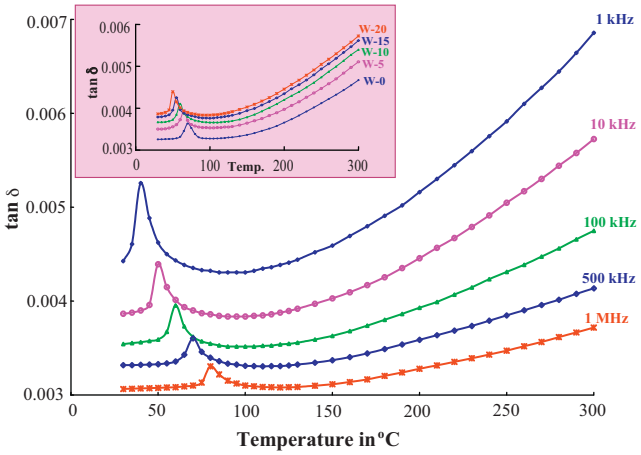

Fig. 7. Variation of dielectric loss $\tan\delta$ of the glass W-20 with temperature at different frequencies. Inset figure gives the variation of $\tan\delta$ with temperature at 10 kHz for different concentrations of WO_3 in ZnO–As_2O_3–Sb_2O_3 glasses.

relaxation curves with increase in the concentration of WO_3 with a shift of the relaxation region towards lower temperature. Using the relation,

$$f = f_o \exp\left(\frac{-W_d}{kT}\right), \quad (2)$$

the effective activation energy, W_d, for the dipoles is calculated; the activation energy is found to be the lowest for the sample W-20. Summary of the data on the relaxation effects of ZAS: WO_3 glasses is presented in Table 5 along with other pertinent data.

The a.c. conductivity $\sigma_{a.c.}$ is calculated at different temperatures using the equation:

$$\sigma_{a.c.} = \omega\,\varepsilon'\,\varepsilon_o \tan\delta, \quad (3)$$

where ε_o is the vacuum dielectric constant) at different frequencies for all the glasses. The variation of conductivity at 500 kHz with $1/T$ is shown in Fig. 8. From these plots, the activation energy for conduction in the high temperature region over which a near linear dependence of $\log\sigma_{a.c.}$ with $1/T$ could be observed is evaluated and presented in Table 6 and variation of the same with the concentration of WO_3 is presented as the inset (a) of Fig. 8. Inset (b) of the same figure gives the variation of $\sigma_{a.c.}$ with $1/T$ at different frequencies of sample W-10; inset (c) gives the variation of $\log\sigma_{a.c.}$ with activation energy for conduction at 100 kHz.

The dielectric breakdown strength for pure ZnO–As_2O_3–Sb_2O_3 glasses at room temperature is determined to be 11.67 kV/cm. With the introduction of WO_3, the value of breakdown strength is found to decrease to a value of 11.19 kV/cm; for further increase in the content of WO_3, the breakdown strength is found to decrease substantially and reached a value of 10.24 kV/cm for the glass containing 20 mol% of WO_3 (Table 5).

Table 5
Data on dielectric loss of ZnO–As_2O_3–Sb_2O_3: WO_3 glasses at 500 kHz.

Glass	$(\tan\delta)_{max}$ $\times(10^{-2})$	Temperature region of relaxation (°C)	Activation energy for dipoles (eV)	Breakdown strength (kV/cm)	Spreading factor β
W-0	0.3176	65–120	1.2719	11.67	0.27
W-5	0.3335	60–108	1.2544	11.19	0.29
W-10	0.3456	57-100	1.2369	10.71	0.32
W-15	0.3519	52–92	1.2193	10.48	0.36
W-20	0.3603	50–87	1.2018	10.24	0.38

Table 6
Pertinent data on a.c. conductivity of $ZnO–As_2O_3–Sb_2O_3$: WO_3 glasses at 100 kHz.

Glass	$\sigma_{a.c.}$ at 50 °C $\times(10^{-9})\,(\Omega\,cm)^{-1}$	$N(E_F)$ in $(10^{20}, eV^{-1}/cm^3)$			Activation energy for conduction $\times(10^{-2})$ (eV)
		Austin–Mott	Butcher–Hyden	Pollak	
W-0	3.21	–	–	–	8.08
W-5	3.62	1.23	0.51	1.25	7.86
W-10	4.00	1.29	0.54	1.31	7.73
W-15	4.35	1.35	0.56	1.37	7.66
W-20	4.58	1.38	0.58	1.40	7.63

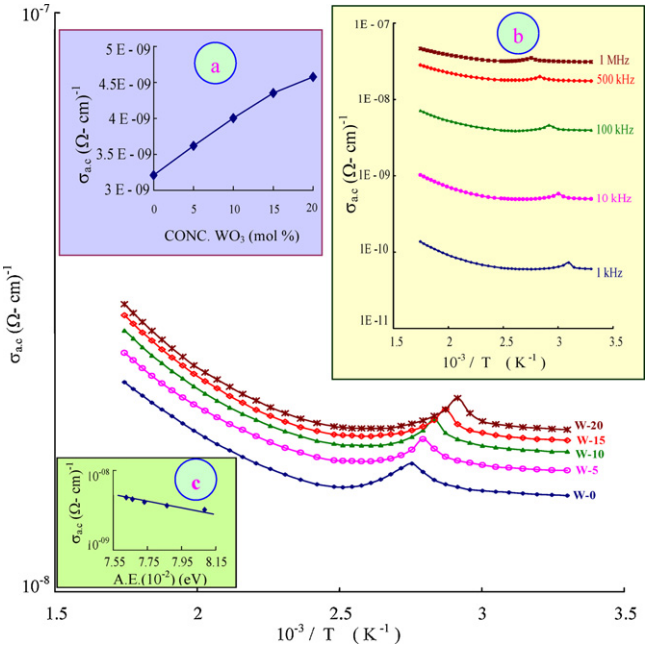

Fig. 8. Variation of $\sigma_{a.c.}$ with $1/T$ at 500 kHz for different concentrations of WO_3 in $ZnO–As_2O_3–Sb_2O_3$ glasses. Inset figures give the variation of (a) $\sigma_{a.c.}$ with the concentration of WO_3 in the ZAS glass matrix, (b) $\sigma_{a.c.}$ with $1/T$ of the glass W-10 at different frequencies and (c) $\log\sigma_{a.c.}$ with activation energy for conduction at 100 kHz.

5. Discussion

In general, the properties of a glass depend upon its composition and to a considerable extent upon its structure. $ZnO–As_2O_3–Sb_2O_3$ glasses containing tungsten oxide have a complex composition and are an admixture of network formers, intermediates and modifiers. As_2O_3 is a strong network former with corner sharing AsO_3 pyramidal units; normal bond lengths of As–O lie between 1.72 and 1.81 Å and O–As–O, As–O–As bond angles lie in the range 90–103°, 123–135° respectively. Sb_2O_3 is an incipient glass network former (and as it does not readily form the glass but do so in presence of modifiers like ZnO). Sb_2O_3 participates in the glass network with triangular SbO_3 pyramids that can be viewed as tetrahedrons with the oxygen at three corners and a lone pair of electrons of antimony (Sb^{3+}) at the fourth corner localized in the third equatorial direction of Sb atom. In the glass network, the Sb–O distances range from 2.0 to 2.6 Å with the coordination number of Sb as 3.0. The coordination polyhedra are joined by sharing corners to form double infinite chains with the lone pairs pointing out from the chains. These chains are held together by weak secondary Sb–O bonds with lengths greater than 2.6 Å. The earlier X-ray diffraction investigations on some Sb_2O_3 glass system indicate that the nearest neighbor Sb–Sb distance is ~3.4 Å with a coordination number of 1.7. The third oxygen in each SbO_3 unit must take part in the linkages of the type Sb–O–As [21–24]. The presence of common meta-centers of υ_2 and υ_3 vibrational bands of As_2O_3 and Sb_2O_3 in the ranges 650–668 cm^{-1} and 770–787 cm^{-1}, respectively, in the IR spectra of present glasses in fact supports the formation of such linkages. ZnO is, in general, a glass modifier and enters the glass network by breaking up the As–O–As, Sb–O–As bonds (normally the oxygens of ZnO break the local symmetries while Zn^{2+} ions occupy interstitial positions) and introduces co-ordinate defects known as dangling bonds along with non-bridging oxygen ions; in this case Zn^{2+} is octahedrally co-ordinated [25,26]. However, ZnO may also participate in the glass network with ZnO_4 structural units when zinc ion is linked to four oxygens in a co-valency bond configuration [27].

WO_3 belongs to the intermediate class of glass forming oxides; it is an incipient glass network former, normally tungsten ion exists in W^{6+} state and participates in glass network withWO_4 and WO_6 structural units and may alternate with antimony and arsenic structural units [28,29]. Further, tungsten ions also seem to exist in present glass matrices in W^{5+} state with $W^{5+}O_3$ complexes (evidenced from ESR and optical absorption spectra) in all the glasses containing WO_3 and are expected to occupy only interstitial positions since the ratio of cation–oxygen radii is 0.45 for W^{5+} ion, which is far from the value of 0.19 possessed by an ion to occupy tetrahedral or substitutional sites [30] and act as modifiers similar to other modifier ions. The WO_4 units are likely alternate with arsenate and antimonite structural groups and form the linkages of the type As–O–W, Sb–O–W (substantiation from IR and Raman spectra).

Recollecting the data on DTA, the values of the glass transition temperature T_g and glass forming ability parameters viz., the ratios $(T_c - T_g)/T_g$, T_g/T_m, $(T_c - T_g)/T_m$ and K_{gl}, have been observed to decrease with increase in the concentration of WO_3. Lower values of these parameters indicate lower thermal stability of the glasses [31]. Normally, the decrease in bond length, cross-link density and closeness of packing of various structural groups in the glass matrix, are responsible for such a decrease of these parameters. The manifestation of these results is that, with the increasing presence of WO_3 in the glass network, tungsten ions seem to exist in W^{5+} state, occupying glass modifier positions similar to Sb^{3+} and Zn^{2+} ions, reduce the cross-link density and weaken the mean bond strength, resulting a decrease in the rigidity of the glass network.

The decrease in the optical band gap with the increasing concentration of WO_3 may be explained as follows: the gradual increase in the concentration of W^{5+} ions, causes a creation of large number of donor centers; subsequently, the excited states of localized electrons originally trapped on W^{5+} sites begin to overlap with the empty 5d states on the neighboring W^{6+} sites. As a result, the impurity band becomes more extended into the main band gap. This development might have shifted the absorption edge to the lower energy which leads up to a significant shrinkage in the band gap as observed. The broad band observed in the optical absorption spectra of the tungsten doped glasses is identified due to $d_{xy} \rightarrow d_{x^2-y^2}$ transition of the W^{5+} ion with crystal field parame-

ters around $\Delta = 16{,}000\,cm^{-1}$ and $\delta = 13{,}000\,cm^{-1}$ [32]. In fact, two optical excitations were predicted starting from d_{xy} ground state, but because of the strong intervalence charge transfer transition between W^{5+} and W^{6+} ions, the two bands could not be resolved in the spectra of $ZnO–Sb_2O_3–As_2O_3$ glasses. However, the increasing intensity and half width of this band with the increasing content of WO_3 in these glasses suggest the growing concentration of W^{5+} ions. Thus, the analysis of optical absorption spectra of these glasses obviously indicates an enhancing degree of depolymerization of the glass network.

The presence of different structural groups in these glasses can be established from the IR spectra (Fig. 3). With the introduction of WO_3 into the ZAS glass matrix, the sudden shift observed in the band of υ_1 vibrations of Sb_2O_3 towards lower wavelength suggests the presence of υ_1 vibrations of WO_4 units in the region (930–941 cm^{-1}) and hence the formation of Sb–O–W linkages [5] in the glass network. However, with the increasing concentration of WO_3, the gradual decrease in the intensity of this band with a simultaneous increase in the intensity of its adjacent band (band due to υ_3 vibrations of WO_6 structural units) indicates the reduction of such linkages in the specimens under study. Thus, IR spectra explores the progressive modifying action of tungsten ions and point out the decreasing network connectivity with the increasing content of WO_3 in the glass network.

In Raman spectra the characteristic bands of the ZAS (W-0) glass are strongly affected by the addition of WO_3. From the spectra it is evident that, an enormous decrease in the intensity of the band in the middle-frequency region at 440 cm^{-1}, ascribed to the symmetric stretching vibrations of AsO_3, SbO_3 and ZnO_4 units (characteristic of the vibrations of bridging oxygen atoms [33] between Zn–As, Zn–Sb and As–Sb units) and the simultaneous increase in the intensity of the band at 938 cm^{-1}, attributed to the asymmetric stretching vibrations of terminal W–O bonds in WO_6 octahedra along with that of the other asymmetric bands suggests a very strong devitrification of the ZAS glass matrix with the increasing content of WO_3 in the glass network.The presence of asymmetric line in the ESR spectra of these glasses is similar to the behavior of nd^1 ions in oxide glasses which form a local C_{4V} symmetry [34]. The values of g factor observed in the range $1.64 < g_\perp < 1.75$ and $1.55 < g_{||} < 1.65$ indicate that W^{5+} ions present in axially distorted octahedral positions with a short W–O bond and an opposite long W–O bond along the symmetry axis of oxygen ions [20]. Further, the highest intensity of the two signals observed in the spectra of the glass W-20 also suggest the highest concentration of W^{5+} ions and O^- ion defect centers in these glasses.Additionally, the difference between $g_{||}$ and $g_\perp$ (anisotropy factor) changes with the concentration of WO_3 in the glass network; this observation indicates that W^{5+} octahedron experiences structural changes with the concentration of WO_3. The values of $k_{||}$ and $k_\perp$ covalent reduction factors of W–O bonds along the z-axis and in the (x, y) plane, respectively, are evaluated using the equations.

$$g_{||} = g_e - \frac{(8k^2{}_{||}\lambda)}{\Delta}, \tag{4}$$

$$g_\perp = g_e - \frac{(2k^2{}_\perp\lambda)}{\delta}, \tag{5}$$

where $g_\perp$ and $g_{||}$ are the g values obtained in the present measurements, g_e is the free electron g factor, λ is the spin–orbit coupling constant and Δ is the energy of $d_{xy} \rightarrow d_{x^2-y^2}$ transition and δ is the splitting due to tetragonal distortion [35]. The values of $k_\perp$ and $k_{||}$ obtained for the $ZnO–As_2O_3–Sb_2O_3$: WO_3 glasses are presented in Table 4; the covalency factor $k_{||}$ characterizes the four-fold symmetry axis. With the increase in the concentration of WO_3 the value of $k_{||}$ increases indicating that W–O bond in the z-direction becomes less covalent. Similarly, the factor $k_\perp$ characterizes four W–O bonds located in (x, y) plane; these bonds are normally more ionic than those in parallel direction. Thus, the analysis of ESR spectra indicates that the ZAS glass matrix gradually looses the covalent character with the increasing concentration of WO_3.

In general, the dielectric constant of a material is due to electronic, ionic, dipolar and space charge polarizations. Out of these, the space charge contribution depends on the purity and perfection of the glasses. Recollecting the data, on dielectric properties of $ZnO–As_2O_3–Sb_2O_3$: WO_3 glasses, a substantial hike in the values of the dielectric parameters (with respect to those of pure glass) is observed with increase in the concentration of WO_3; such an increase is obviously due to the presence of larger concentration of W^{5+} ions that act as modifiers similar to Zn^{2+} ions and generate bonding defects by breaking the As–O–As, Sb–O–As bonds. The defects thus produced create easy pathways for the migration of charges that would build up space charge polarization and lead to an increase in the dielectric parameters as observed [36–38].

The way the dielectric constant and the loss vary with the frequency and temperature (Figs. 6 and 7) suggests that all these glasses exhibit dielectric relaxation effects. Conventionally, the dielectric relaxation effects are described with the variable frequency at a fixed temperature. However, similar information can also be obtained by analyzing these results at a fixed frequency with variable temperature by a pseudo Cole–Cole plot method as suggested by Bottcher and Bordewijk [39]. According to this method the plot between $\varepsilon'(T)$ and $\varepsilon''(T)$ (pseudo Cole–Cole plot), cuts ε'-axis at ε_s and ε_∞. Here, ε_s is known as high temperature dielectric constant (in contrast to the low frequency dielectric constant in the conventional Cole–Cole plot) and similarly ε_∞ is the low temperature dielectric constant. The plot cuts ε'-axis at an angle of $(\pi/2)\beta$ at low temperature side (as per Sixou), here β is the spreading factor for relaxation times. Such plots have been drawn for all the glasses and the value of β is estimated; the value of β is found to increase gradually when the concentration of WO_3 is raised in the glass matrix (Table 5). Thus, the analysis indicates that there are different types of dipoles that are contributing to the relaxation effects in these glasses. Normally, the divalent ions like Zn^{2+} ions with the association of cationic vacancies do exhibit relaxation effects. Earlier studies on the glasses containing d^1 ions like V^{4+}, Cr^{5+}, Ti^{3+}, Mo^{5+} and also W^{5+} showed that these ions contribute to the dielectric relaxation effects [40–42]; hence, the observed relaxation effects and their spreading in the present glasses can safely be attributed to W^{5+} ions. The shifting of relaxation region towards lower temperatures and decrease in the activation energy for the dipoles with increase in the concentration of WO_3 (Table 5) suggests an increasing degree of freedom for dipoles to orient in the field direction in the glass network and thus point out the decreasing rigidity of the glass network with increase in the concentration of WO_3.

When a plot is made between $\log\sigma(\omega)$ vs. activation energy for conduction (in the high temperature) a near linear relationship is observed (inset (c) of Fig. 8); the near linearity between the conductivity and activation energy suggests the conductivity enhancement is directly related to the increasing mobility of the charge carriers in the high temperature region. Further, the variation of conductivity in high temperature region with the concentration of tungsten ions shows an increasing trend; such a trend suggests that it is quite unlikely that the conduction in this region to be connected with the ionic motion [36,43].

The low temperature part of the conductivity (a near temperature independent part, as in the case of present glasses up to nearly 50 °C) can be explained on the basis of quantum mechanical tunneling model (QMT) [44] as in the case of many other glass systems reported recently [45–47]. The value of $N(E_F)$ i.e. the density of

the defect energy states near the Fermi level, evaluated using the equation [44]

$$\sigma(\omega) = \eta e^2 kT[N(E_F)]^2\,\alpha^{-5}\omega\left[\left(\frac{\ln(\nu_{ph}}{\omega}\right)\right]^4, \quad (6)$$

where $\eta = \pi/3$ (Austin and Mott [44]), $= 3.66\pi^2/6$ (Butcher and Hyden [48]), $= \pi^4/96$ (Pollak [49]), with the usual meaning of the symbols reported in the earlier paper [50] and furnished in Table 6. The value of $N(E_F)$ is found to increase with increasing concentration of tungsten ions, indicating an increasing degree of disorder in the glass network.

With the addition of WO_3 to the ZAS glass matrix, we have observed a substantial decrease in the value of dielectric breakdown strength (Table 5). When a dielectric is placed in the electric field, the heat of dielectric loss is liberated. If the applied field is an alternating field, the specific dielectric loss, i.e., the loss per unit volume of the dielectric is given by [51]

$$\rho_1 = E^2\omega\varepsilon_0\varepsilon' \tan\delta\ \mathrm{W/m^3}. \quad (7)$$

This equation indicates that higher the values of $\varepsilon' \tan\delta$ of the glass at a given frequency, higher are the values of ρ_1. In a dielectric across which the voltage is applied, heat is liberated, the temperature of the dielectric then raises and the loss increases still more. The dielectric breakdown strength is, in fact, inversely proportional to the specific dielectric loss represented by Eq. (7).

Our observations on breakdown strengths of $ZnO–As_2O_3–Sb_2O_3$: WO_3 glasses, as mentioned earlier, indicate the rate of increase of $\varepsilon' \tan\delta$ with temperature is the highest for glass W-20. Though the breakdown strengths are actually determined at room temperature, the heat liberated during the breakdown, raises the temperature of the glass and hence raises the $\varepsilon' \tan\delta$ value. Thus, the experiments on the dielectric breakdown strength also reveal that the tungsten ions in ZAS glasses mostly exist in pentavalent state, occupying glass lattice modifier positions and cause the conductivity to increase.

6. Conclusions

The conclusions drawn from the study of various properties of $ZnO–As_2O_3–Sb_2O_3$ glasses doped with different concentrations of WO_3 are summarized below:

1. DTA results point out the decreasing glass forming ability of the ZAS glass matrix with the addition of WO_3.
2. The spectroscopic studies indicate that with the increasing content of WO_3 part of the W^{6+} ions in these glasses get converted into W^{5+} ions and thereby cause the strong depolymerization of arsenate and antimonite units leading to an increasing structural disorder in the glass network.
3. The dielectric properties specify that increasing concentration of WO_3 in these glasses directs most of the tungsten ions to occupy octahedral positions with $W^{5+}O_3^-$ complexes, resulting substantial hike in the conductivity and devitrifies the zinc arsenic antimony glass network.

Thus, a strong degree of deformation in the glass network appears in the studied ZAS glasses with the addition of WO_3.

References

[1] Gaël Poirier, Fábia C. Cassanjes, Younes Messaddeq, Sidney J.L. Ribeiro, J. Non-Cryst. Solids 355 (2009) 441.
[2] C. Lasbrugnas, P. Thomas, O. Masson, J.C. Champarnaud-Mesjard, E. Fargin, V. Rodriguez, M. Lahaye, Opt. Mater. 31 (2009) 775.
[3] Y.B. Saddeek, Philos. Magn. 89 (2009) 41.
[4] A. Sheoran, S. Sanghi, S. Rani, A. Agarwal, V.P. Seth, J. Alloys Compd. 475 (2009) 804.
[5] Y. Gandhi, K.S.V. Sudhakar, M. Nagarjuna, N. Veeraiah, J. Alloys Compd. 485 (2009) 876.
[6] G. Bianca Montanari, Anne J. Barbosa, Sidney J.L. Ribeiro, Younes Messaddeq, Gaël Poirier, Máximo S. Li, Appl. Surf. Sci. 254 (2008) 5552.
[7] E.B. Intyushin, V.A. Novikov, Thin Solid Films 516 (2008) 4194.
[8] V. Dimitrov, M. Arnaudov, Y. Dimitriev, Monatsh. Chem. (Chem. Monthly) 115 (1984) 987.
[9] R.M. Abdelouhab, R. Braunstein, K. Barner, J. Non-Cryst. Solids 108 (1989) 109.
[10] K. Nassau, D.L. Chadwick, A.E. Miller, J. Non-Cryst. Solids 93 (1987) 115.
[11] G.N. Papatheodorou, S.A. Solin, Phys. Rev. B 13 (1976) 1741.
[12] M. Bouchard, D.C. Smith, Spectrochim. Acta A 59 (2003) 2247.
[13] H.S. Liu, T.S. Chin, Phys. Chem. Glasses 38 (1997) 123.
[14] H.J. Becher, J. Less-Common Met. 76 (1980) 169.
[15] T. Sekiya, N. Mochida, S. Ogawa, J. Non-Cryst. Solids 176 (1994) 105.
[16] P. Cailet, P. Saumagne, J. Mol. Struct. 4 (1969) 191.
[17] F. Knee, R.A. Condrate Sr., J. Phys. Chem. Solids 40 (1969) 351.
[18] M.S. Augsburger, J.C. Pedregosa, J. Phys. Chem. Solids 56 (8) (1995) 1081.
[19] J. Hanuza, L. Macalik, M. Maczka, E.T.G. Lutz, J.H. Vander Mass, J. Mol. Struct. 511 (1999) 85.
[20] Lee Sook, P.J. Bray, J. Chem. Phys. 39 (1963) 2863;
Lee Sook, P.J. Bray, J. Chem. Phys 40 (1964) 2982.
[21] K. Muruganandam, M. Seshasayee, Phys. Chem. Glasses 40 (1999) 287.
[22] B. Dubois, J.J. Videau, M. Couzi, J. Portier, J. Non-Cryst. Solids 88 (1986) 355.
[23] P.J. Miller, C.A. Cody, Spectrodum. Acta Crystallogr. A 38 (1982) 555.
[24] T.S. Honma, R. Sato, Y. Benino, T. Komastu, V. Dimitrov, J. Non-Cryst. Solids 272 (2000) 1.
[25] M.R. Reddy, S.B. Raju, N. Veeraiah, Bull. Mater. Sci. 24 (2001) 63.
[26] M.R. Reddy, S.B. Raju, N. Veeraiah, J. Phys. Chem. Solids 61 (2000) 1567.
[27] P. Subbalakshmi, N. Veeraiah, Ind. J. Eng. Mater. Sci. 8 (2001) 275.
[28] A.A. Bhagat, M.M. El-Samanoudy, J. Phys. Chem. Solids 60 (1999) 1921.
[29] G. Poirier, M. Poulain, Y. Messaddeq, S.J.L. Ribeiro, J. Non-Cryst. Solids 351 (2005) 293.
[30] S.M.D. Nery, W.M. Pontuschka, S. Isotani, C.G. Rouse, Phys. Rev. B 49 (1994) 3760.
[31] V. Simon, D. Muresan, A.F. Takács, M. Neumann, S. Simon, Solid State Ionics 178 (2007) 221.
[32] M. Von Dirke, S. Muller, K. Barner, H. Rager, J. Non-Cryst. Solids 124 (1990) 265.
[33] L. Koudelka, J. Subcik, P. Mosner, L. Montagne, L. Delevoye, J. Non-Cryst. Solids 353 (2007) 1828.
[34] A. Goldstein, V. Chiriac, D. Becherescu, J. Non-Cryst. Solids 92 (1987) 271.
[35] R.R. Rakhimov, D.E. Jones, H.L. Rocha, A.I. Prokof'ev, A.I. Aleksandrov, J. Phys. Chem. B 104 (2000) 10973.
[36] S. Bala Murali Krishna, A. Ramesh Babu, Ch. Rajya Sree, D. Krishna Rao, J. Non-Cryst. Solids 356 (2010) 1754.
[37] A.K. Maity, J. Electro-Chem. Soc. 152 (2005) 94.
[38] L. Srinivasa Rao, M. Srinivasa Reddy, M. Rami Reddy, N. Veeraiah, J. Alloy. Compd. 464 (2008) 472.
[39] C.J.F. Bottcher, P. Bordewijk, Theory of Electric Polarization, Elsevier, Oxford, 1978.
[40] R.M. Abdelouhab, R. Braunstein, K. Baerner, J. Non-Cryst. Solids 108 (1989) 109.
[41] P. Syam Prasad, M. Srinivasa Reddy, V. Ravi Kumar, N. Veeraiah, Philos. Magn. 87 (2007) 5763.
[42] M. Srinivasa Reddy, V.L.N.S. Raja, N. Veeraiah, EPJ Appl. Phys. 37 (2007) 203.
[43] B. Roling, M.D. Ingram, J. Non-Cryst. Solids 265 (2002) 113.
[44] I.G. Austin, N.F. Mott, Adv. Phys. 18 (1969) 657.
[45] G. Srinivasa Rao, N. Veeraiah, Eur. Phys. J. Appl. Phys. 16 (2001) 11.
[46] G. Venkateswara Rao, N. Veeraiah, J. Alloys Compd. 339 (2002) 54.
[47] A.V. Rao, N. Veeraiah, J. Phys. Chem. Solids 67 (2006) 2263.
[48] P. Butcher, K.J. Hyden, Philos. Magn. 36 (1997) 657.
[49] M. Pollak, Philos. Magn. 23 (1971) 579.
[50] S.V.G.V.A. Prasad, G. Sahaya Baskaran, N. Veeraiah, Phys. Status Solidi A 202 (2005) 2812.
[51] B. Tareev, Physics of Dielectric Materials, Mir Publishers, Moscow, 1979.